

Banner appropriate to article type will appear here in typeset article

Baroclinic Tidal Conversion: Note on a Paper of L. R. M. Maas

Carl Wunsch¹†, and Jared Wunsch²

¹Department of Earth and Planetary Sciences, Harvard University, Cambridge MA 02138, US

²Department of Mathematics, Northwestern University, Evanston IL 60208, US

(Received xx; revised xx; accepted xx)

Maas (2011) showed that for an oscillating two-dimensional barotropic tide flowing over sub-critical topography of compact support, some topographic forms existed that produced non-radiating baroclinic disturbances. The problem is related to “stealth” and “cloaking” problems. Here Maas’s result is derived using a simpler approach, not involving complicated mappings, but formally restricted to perturbation topography. Wider results come from the discussion of nearly-compact support topographic disturbances provided by Schwartz functions with weak high-wavenumber radiation and by exploiting both a known functional equation formulation and Fourier methods. The problem is extended to disturbances on uniform slopes. A variety of non-radiating topographies can be found, although they are mathematically delicate and unlikely to be found in nature. Topography with weak radiation at high wavenumber is a much wider class of structures. Application of these solutions would lie with the ability to estimate dissipation over and near the topography from motions observed at a distance.

1. Introduction

Early interest in the conversion of the barotropic tide into baroclinic (linear inviscid internal wave) modes can be found in the papers of Cox and Sandstrom (1962) and Baines (1973). Garrett and Kunze (2007) reviewed work to that date, the major progress having come after the global detection of internal tides in altimetric data (Ray and Mitchum, 1997). Numerous later papers have dealt with various methods, topographies, and physics including nonlinearities. Morozov (2018) is a monograph on the subject with a focus on in situ observations. The importance of the problem arises from the major tidal contribution to the energy budget controlling ocean mixing and evolution of the lunar orbit.

Maas (2011) (cf. also Magaard (1962)) showed, surprisingly, that two-dimensional bottom topography shapes existed in which zero conversion occurred, as though the bottom topography were transparent to an incoming barotropic flow (and see the commentary by Llewellyn Smith, 2011). Earlier, Sandstrom (1975), using a different approach, had shown the existence of such configurations (his Table 1). Some care is required concerning the assertion in the previous sentences because a disturbance, trapped to the topography, does exist and it will be dissipative and non-linearly radiating, but no radiating baroclinic flow occurs in the linear problem.

† Email address for correspondence: jwunsch@math.northwestern.edu

This present note arose initially from an attempt to formulate an inverse theory perspective, for which two interesting, if hypothetical, questions emerge: (1) Can measurement of near- or far-fields of internal waves be used to reconstruct the generating topography? (2) How does a non-radiating topography emerge as a solution in an inverse calculation (a null space)? The problem is reminiscent of the one called ‘Can you hear the shape of a drum?’ (Kac, 1966, Gordon and Webb, 1996) directed at determining an unknown boundary shape.

More familiar, analogous, problems are the wave scattering and antenna radiation problems of physics and radio engineering. With the structure of an antenna known, the near-field radiation can be extremely complicated. But as the distance to the antenna increases, much of the complexity vanishes, being trapped in the near-field, and distant patterns are often simplified into dipole and multi-pole patterns. The crucial feature is that much of the structure in the near-field is non-propagating, and so the far-field is simplified (e.g. Stratton, 1941, p. 435). On the other hand, measurements in the far-field then cannot be used to reconstruct the near-field pattern, a desirable feature in the problem of radar cross-section reduction in “stealth” technology (e.g. Bahret, 1993) or in the wider field of “cloaking” (Kadec et al., 2015).

Maas (2011, hereafter M11) and Maas and Harlander (2011) used an analogue of conformal mapping for solving the hyperbolic-in-space equation governing the internal wave field. The resulting transformation does not have a physically obvious interpretation even in the linearized case, and the main point of this present note is to show that a more direct mathematical approach suffices in the case of perturbative topography considered here. Sandstrom’s (1975) solution in terms of characteristics is also physically more accessible. The general problem of understanding the effectiveness of baroclinic tidal generation for any given topographic structure here remains the central theme.

A partial differential equation hyperbolic in space (Eq. 1 below) generates a number of fascinating mathematical problems including extreme sensitivity to the boundary conditions describing the topography. From a physical standpoint however, many of the mathematical issues are likely irrelevant, at least on some scales: the hyperbolic character in this problem arises from the reduction in the order of the equation from a system including viscosity and diffusion. These processes raise the order of the system and suppress the hyperbolic characteristic curves of the reduced system in the high-wavenumber regime. Wunsch (1969) included a brief discussion of the boundary-layer on a uniform slope in the fourth-order frictional system. Unlike some other problems, strong dissipative properties are not restricted to boundary layers at walls—the existence of discontinuous interior (super-critical) solutions to Eq. (1) below implies that those processes can act intensely throughout the fluid volume. The existence of fluid interior as well as boundary dissipation suggests that a modal approach will be more robust than method-of-characteristics solutions. Reduction into low modes in the far-field is consistent with ocean observations (e.g., Zhao et al. 2016), whereas long-distance propagation of identifiable characteristics is not; admittedly, however, the currently available satellite data is not well adapted to observation of transient, high-wavenumber phenomena.

2. Governing Equation

In Cartesian coordinates, the equation governing the stream function, $\psi(x, z)$, for inviscid, two-dimensional, linear internal wave propagation of frequency ω in a uniformly stratified fluid (constant buoyancy frequency, N , and Coriolis frequency, $f_0 < N$) is the hyperbolic-in-space Poincaré or Poincaré-Sobolev equation ,

$$\frac{1}{c^2} \frac{\partial^2 \psi}{\partial x^2} - \frac{\partial^2 \psi}{\partial z^2} = 0, \quad c^2 = \frac{\omega^2 - f_0^2}{N^2 - \omega^2} > 0, \quad c > 0 \quad (2.1)$$

in a channel of depth $h(x)$ as here, or in an infinitely deep ocean, $-\infty < z \leq h$. A factor $\exp(-i\omega t)$ is implicit. The velocity field, $\mathbf{u} = (u, w)$,

$$u = \frac{\partial \psi}{\partial z}, \quad w = -\frac{\partial \psi}{\partial x},$$

is subject to a top boundary condition of $w = 0$ and a bottom boundary condition of $\mathbf{u} \cdot \nabla(h - z) = 0$, i.e. no normal flow. If $c^2 < 0$, that is, $\omega^2 > N^2$ or $\omega^2 < f_0^2$, the nature of the equation changes from hyperbolic to elliptic. This latter regime, particularly important for diurnal and longer period tidal forcing poleward of about 30° latitude, is of considerable oceanographic interest, but is not discussed here. When $\omega^2/N^2 \rightarrow 0$, the system is hydrostatic. Llewellyn Smith and Young (2006) described the important role of a finite, reflective, upper boundary relative to an infinitely deep ocean.

Eq. (2.1) has been written so that if t (time) is substituted for x , the equation has the same form as an ordinary one-dimensional wave equation with wave speed c . In such problems, a boundary that moves faster than c would generate a shock, or be physically impossible if c is the speed of light (see, e.g., Balazs, 1961 or Greenspan, 1963). These problems require causality in the x, t domain, but no such causality is required in x, z where information can flow ‘backwards’ in x . As is well-known, the internal wave problem can be divided into regimes according to the topographic slope. Here we consider the regime with slopes γ that are sufficiently shallow ($\gamma < c$) that no non-causal characteristics are generated by reflection of causal characteristics off the topography. Such slopes are labelled ‘transmissive’ or ‘subcritical’ meaning that energy (information) is *not* returned in the direction in x from which the disturbance originated. By contrast, when slopes are sufficiently large ($\gamma > c$), non-causal characteristics can exist; these slopes are ‘reflective’ or ‘super-critical.’ Poincaré (1885) discussed the corresponding spatially hyperbolic equation for the interior of an unstratified, $N = 0$, but strongly rotating, fluid container. As a ‘critical’ slope, $\gamma = c$, is approached, the characteristic curves become tangent to the boundary, and solution infinities are generated. What follows is restricted to the transmissive, subcritical, case.

From here, the notation differs slightly from that in M11: the z -coordinate origin is taken at constant reference depth, h , so that the upper rigid lid is at $z = h$. The most natural spatial scale comes from the water depth, so that a non-dimensional vertical coordinate, z^* is defined as $z = hz^*$ and the non-dimensional horizontal coordinate is defined as $x = hx^*/c$. The upper lid is at $z^* = 1$ and the disturbance to the seafloor about $z = 0$ is $z = h_1(x/h)$ or $z^* = h_1(x^*/c)/h \ll 1$. Eq. (2.1) becomes,

$$\frac{\partial^2 \psi^*}{c^{*2} \partial x^{*2}} - \frac{\partial^2 \psi^*}{\partial z^{*2}} = 0, \quad c^* = 1; \quad (2.2)$$

c^* is retained as a mnemonic device. With a flat bottom, the dimensional forced oscillatory solution to Eq. (2.1) consists of a uniform horizontal flow,

$$\psi_0(z) = Uz, \quad (2.3)$$

and non-dimensional ψ is defined from $\psi = (Uh)\psi^*$. Flow is left-to-right when $U > 0$, although oscillating in direction with t . Choose $U = 1$.

At this point, the $*$ will be dropped, all variables being non-dimensional. The role of c is as a reminder that the *horizontal* scale will change with the frequency of oscillation. With a flat bottom, in addition to ψ_0 , an infinite set of internal wave modes exists,

$$\psi_{iw} = \sum_{m=-\infty}^{\infty} A_m e^{\pi i m c x} \sin(m\pi z), \quad (2.4)$$

all satisfying the two Dirichlet boundary conditions $\psi(z = 0, z = 1) = 0$, and which radiate

to and from infinity in $\pm x$. Periodicity in cx is 2. For these vertically-standing modes, zonal phase and group velocities are in the same direction.

Assume now that a non-zero value of $\psi_0 = z$ is imposed in the channel with a perturbation $h_1(cx)$ to the bottom boundary, so that the non-dimensional bottom boundary condition is linearized about $z = 0$ with $U = 1$:

$$(u, w) \cdot \nabla(h - z) = \frac{\partial h_1}{\partial(cx)} - w(z = 0) = 0. \quad (2.5)$$

Balmforth et al. (2002), Pétrélis et al. (2006) and a number of other authors provided examples of what is considered the ‘forward’ or ‘direct’ problem for ψ , given $h_1(cx)$. When $\partial h_1(cx)/\partial(cx) < 1$, the slope is subcritical. In an infinite channel as discussed here, radiation conditions must usually be imposed as $|cx| \rightarrow \infty$. (A finite amplitude case is considered briefly at the end.)

3. Simplified Solution

Consider, in non-dimensional space, subcritical, transmissive, topography, $h_1(cx)$, with the boundary condition linearized about $z = 0$. Let

$$\psi = f(cx - z + \alpha_1) + g(cx + z + \alpha_2)$$

f, g are arbitrary, but twice differentiable, solutions to Eq. (2.2), where α_i are constants. On $z = 1$, $f(cx - 1 + \alpha_1) = -g(cx + 1 + \alpha_2)$, and choosing $\alpha_1 = 1$, $\alpha_2 = -1$ (in effect, using the method of images), $g(q) = -f(q)$. Then,

$$\psi(cx, z) = f(cx - z + 1) - f(cx + z - 1), \quad -\infty \leq x \leq \infty, \quad (3.1)$$

satisfying the upper boundary condition, $\psi(z = 1) = 0$ (see Manton and Mysak, 1971; Bühler and Holmes Cerfon, 2011).

If the difference in Eq. (3.1) is non-zero only inside some interval P , effectively vanishing outside $x \in P$, then no far-field radiation will be generated. Following mathematical practice, functions with that confined support will be called ‘rapidly decreasing functions’ (RDF); see Cheney (2001). If no far-field disturbance occurs, then radiation conditions (RC) become irrelevant.

The perturbation vertical velocity is,

$$w(cx, z) = -\frac{\partial \psi}{\partial(cx)} = -f'(cx - z + 1) + f'(cx + z - 1), \quad (3.2)$$

and setting

$$w(cx, 0) = -f'(cx + 1) + f'(cx - 1) = \frac{\partial h_1}{\partial(cx)}, \quad (3.3)$$

or

$$-f(cx + 1) + f(cx - 1) = h_1(cx) + H, \quad (3.4)$$

with H arbitrary and set to zero. $h_1(cx)$ will be RDF if the difference in Eq. (3.4) is RDF even if $f(cx)$ is not itself RDF. Any $f(cx)$ of period 2 (the usual non-RDF Eq. (2.4) flat-bottom radiating free modes) can be added to the solution f , without necessitating a change in h_1 .

Note that nonradiating examples are easy to come by: we may freely specify f a function of rapid decrease, and then simply set

$$h_1(cx) = f(cx - 1) - f(cx + 1) \quad (3.5)$$

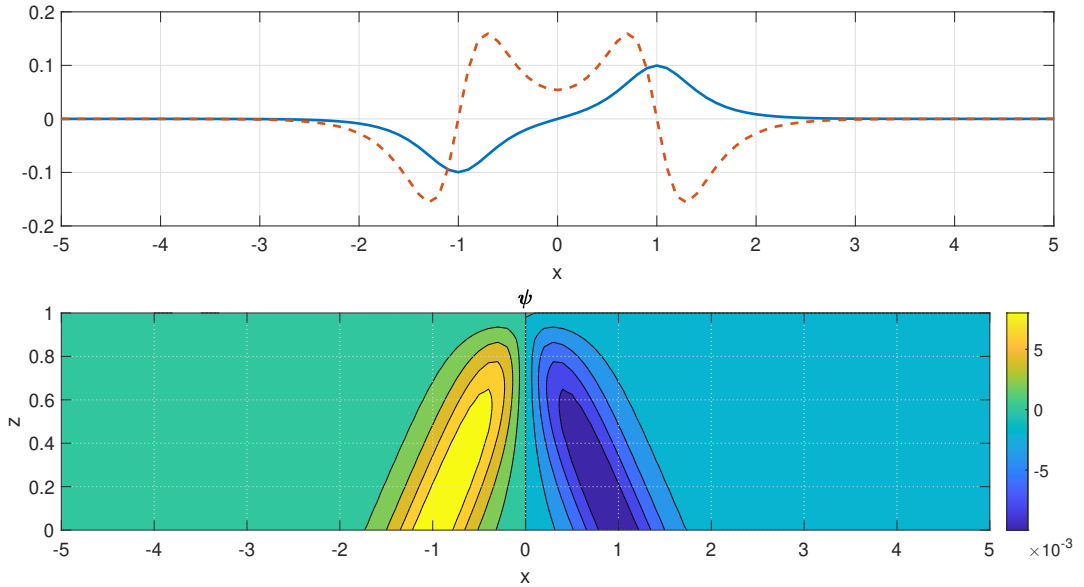


Figure 1: Topography (upper panel) and its derivative (dashed line) and the solution (lower panel), $\psi(x, z)$ in Eq. 3.8. Here $c = 1, \varepsilon = 0.1$. No far-field radiation occurs.

to obtain the topography, and recover ψ from (3.1), which inherits rapid decay (in x) from f . An explicit example of this construction is as follows:

Let

$$f(cx) = \varepsilon \operatorname{sech}(\pi cx) \quad (3.6)$$

$$f'(cx) = -\pi \varepsilon \operatorname{sech}(\pi cx) \tanh(\pi cx), \quad (3.7)$$

then

$$\psi = \varepsilon [\operatorname{sech} \pi(cx - z + 1) - \operatorname{sech} \pi(cx + z - 1)] \quad (3.8)$$

which is exponentially confined to the topography with no radiation. Here and elsewhere, ε is a small parameter. Also,

$$w = \pi \varepsilon [\operatorname{sech} \pi(cx - z + 1) \tanh \pi(cx - z + 1) - \operatorname{sech} \pi(cx + z - 1) \tanh \pi(cx + z - 1)] \quad (3.9)$$

$$h_1(cx) = \varepsilon [-\operatorname{sech}(\pi(cx + 1)) + \operatorname{sech} \pi(cx - 1)] \quad (3.10)$$

$$h_1'(cx) = \pi \varepsilon [\operatorname{sech}(\pi(cx + 1)) \tanh(\pi(cx + 1)) - \operatorname{sech} \pi(cx - 1) \tanh \pi(cx - 1)] \quad (3.11)$$

is the corresponding topography determined inversely from the solution. The flow and topography for $\varepsilon = 0.1$ can be seen in Fig. 1, 2 where $h_1(cx)$ becomes constant and hence non-radiating.

This ‘non-converting’ or ‘non-radiating’ field was called, in M11, the ‘non-hydrostatic barotropic’ flow. But given the numerous conflicting definitions of ‘barotropic’ in the literature, the terminology is avoided here.

In an oceanographic context, the possible existence of such trapped solutions implies a relatively high shear, and hence strong mixing over topographic features. A far-field

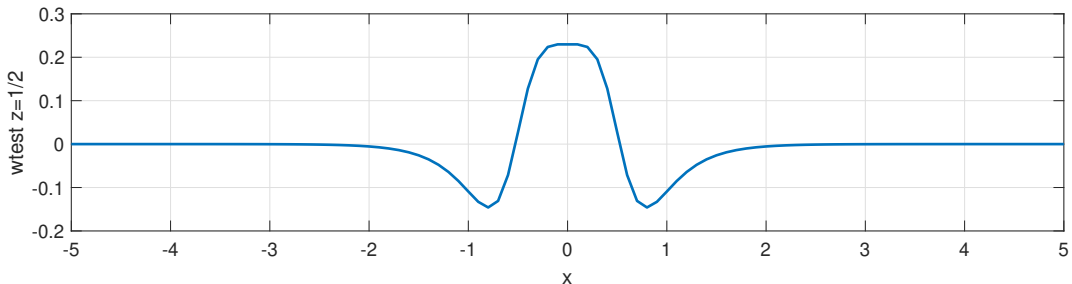


Figure 2: $w(x, z = 1/2) = -\partial\psi/\partial x$, for the double sech bottom profile.

measurement of the resulting disturbance would vanish, and no information about the shear would be recoverable directly. (Indirect estimates might be possible through the influence of a strong mixing region on the larger-scale flow field.)

4. Some Generalization

The label ‘compact support’ implies a function that is identically zero outside an interval P . Such functions f , or topographies, h_1 , do not exist in the real world unless entire ocean basins are considered, and then lateral boundary conditions intrude. Within the class of RDF, ‘bump’ functions are identically zero outside P , and the ‘Schwartz functions’[†] are RDF but are also perfectly smooth (infinitely differentiable), with all derivatives also enjoying rapid decay. For what follows, the most important characteristic of Schwartz functions in wavenumber space is that their Fourier transforms are also Schwartz functions. Rapidity of decay is still subject to the uncertainty principle, however, so that bandwidth in one domain is inversely proportional to that in the other.

To the extent that the wavenumber decay is proportional to a power of k^{-p} , and viscous decay is proportional of $\nabla^2(u, v, w)$, the value p will determine the relative importance of high wavenumber dissipation. Thus if $p = 2$, dissipation is uniform in k ; and larger values of p will tend to minimize high wavenumber contributions to dissipation.

As above, given $f(cx)$ from a known $\psi(cx, z)$, then in a simple formal inverse problem, $h_1(cx)$ is easily determined: the solution is known, and the boundary shape, $h_1(cx)$, is found by subtraction. The Appendix briefly summarizes a situation of practical observations, including noise.

Here the conventional wave generation ‘forward’ problem: for given $h_1(cx)$, find $f'(cx)$, is more interesting, both with and without an RDF requirement. Eq. (3.4) is an innocuous-seeming functional equation examined by Manton and Mysak (1971) and more recently by Beckebanze and Keady (2016), the latter emphasizing closed containers without RC.[‡] Hazewinkel et al. (2010) discuss the application of wave attractors to similar problems. Colin de Verdière and Saint-Raymond (2020) and Dyatlov and Zworski (2019) have recently revisited the analysis of attractors via methods of microlocal analysis. If the RDF requirement is abandoned, Eq. (3.4) provides a general relationship between any perturbation topography and a function f , but *only insofar as RC are satisfied*—and which is not so easily accomplished in general. On the other hand, if ψ has compact support, radiation conditions are irrelevant.

[†] “Good” functions in the terminology of Lighthill (1958) and others.

[‡] Aczél (1966) is a general discussion of functional equations.

4.1. Functional Equation by Operator Inversion

As a linear inverse model, Eq. (3.4) is a very simple one for determining $h_1(cx)$ from $\psi(cx, z)$. In practice, the most common measurement would be of the density/temperature, which is in the linear internal wave theory proportional to $\partial\psi/\partial(cx)$ for any value of cx, z . For any full formulation, sufficient measurements would need to be available to determine not only the trapped components, but also the propagating mode amplitudes.

Here we address the slightly more challenging forward problem of determining $\psi(cx, z)$ given topography h_1 . One form of the ill-posed forward problem solution that complements the above can be described as follows, at least formally. Define the unit backward displacement operator and its inverse,

$$\mathcal{D}_1(g(x)) = g(x - 1) \quad (4.1)$$

$$\mathcal{D}_1^{-1}(g(x)) = g(x + 1) \quad (4.2)$$

Then Eq. (3.3) is

$$\mathcal{D}_1 f'(cx) - \mathcal{D}_1^{-1} f'(cx) = h'_1(cx) \quad (4.3)$$

or

$$\begin{aligned} (\mathcal{D}_1^2 - 1)f'(cx) &= \mathcal{D}_1 h'_1(cx), \text{ and} \\ (1 - \mathcal{D}_1^{-2})f'(cx) &= \mathcal{D}_1^{-1} h'_1(cx) \end{aligned} \quad (4.4)$$

Adding the two forms in Eq. (4.4) and by formal inversion of the operators $(1 - \mathcal{D}_1^2)$, $(1 - \mathcal{D}_1^{-2})$

$$f'(cx) = -\frac{1}{2}(\mathcal{D}_1 + \mathcal{D}_1^3 + \mathcal{D}_1^5 + \mathcal{D}_1^7 + \dots)h'_1(cx) \quad (4.5)$$

$$\begin{aligned} &+ \frac{1}{2}(\mathcal{D}_1^{-1} + \mathcal{D}_1^{-3} + \mathcal{D}_1^{-5} + \mathcal{D}_1^{-7} + \dots)h'_1(cx) \\ &= \frac{1}{2} \sum_{j=0}^{\infty} (h'_1(cx + 2j + 1) - h'_1(cx - 2j - 1)), \end{aligned} \quad (4.6)$$

a sum of the slopes at distances 2 which converges provided $|h'_1(cx)| \leq C/|x|^{1+\epsilon}$ for some $\epsilon > 0$, and producing an explicit solution to the forward problem. The operators $(\mathcal{D}_1^2 - 1)$, $(1 - \mathcal{D}_1^{-2})$ have a null space of any period-2 function in cx , hence the solution f' obtained here is certainly not unique. Note that if the topography is symmetric about $x = 0$ then $h'_1(2j + 1) = -h'_1(-2j - 1)$.

From this perspective if we revisit the construction of nonradiating examples by first specifying f (decaying or compactly supported) and then obtaining h_1 by (3.5), we see that we obtain cancellations in the series (4.5). In particular, let $p(x)$ be any function of compact support. Setting

$$h'_1(cx) = p(cx + 1) - p(cx - 1), \quad (4.7)$$

then the f' series telescopes, with the sum thus having compact support, and the topography is again seen to be non-radiating. Eq. (4.5) provides an especially convenient characterization of the statistics of $f(cx)$ should the topographic slopes be treated as a random process. We remark that while our derivation by operator inversion was purely formal, the resulting manifestly solves the functional equation *ex post facto*, whenever it converges (either pointwise or in the sense of generalized functions).

4.2. Functional Equation By Fourier Methods

We may alternatively give formal solutions to the forward problem of obtaining f from h_1 by Fourier methods. Suppose, in Eq. (3.4), $h_1(cx)$ is RDF. Let

$$h_1(cx) = \int_{-\infty}^{\infty} \hat{h}_1(k) \exp(2\pi i k c x) dk, \quad f(cx) = \int_{-\infty}^{\infty} \hat{f}(k) \exp(2\pi i k c x) dk \quad (4.8)$$

using the conventions of Bracewell (1978). Then,

$$\int_{-\infty}^{\infty} \hat{f}(k) \exp(2\pi i k (cx + 1)) - \hat{f}(k) \exp(2\pi i k (cx - 1)) dk = \int_{-\infty}^{\infty} \hat{h}_1(k) \exp(2\pi i k c x) dk \quad (4.9)$$

That is, there is a solution f given by

$$\hat{f}(k) = \frac{i\hat{h}_1(k)}{2 \sin(2\pi k)}, \quad (4.10)$$

provided the quotient on the right is appropriately interpreted in the sense of the theory of distributions. In general, we thus obtain poles of \hat{f} on the real axis at all $k = n/2$, i.e. at half-integers. Now assume analyticity of $\hat{h}_1(k)$ in the upper-half-plane together with appropriate decay to close the contour of integration; moreover, let us make sense of the quotient by regularizing the resulting integral across the poles of \hat{f} arising in the formal inverse Fourier transform by treating it as a principal value integral at each pole. Thus when inverting for $f(cx)$ we thus obtain the sum of half the corresponding residues, hence formally

$$f(x) = -\pi \sum_{n=-\infty}^{\infty} \hat{h}_1(n/2) \exp(-in\pi c x). \quad (4.11)$$

$$\psi(x, z) = \pi \sum_{n=-\infty}^{\infty} \frac{\hat{h}_1(n/2)}{(-1)^n} [-\exp(-in\pi(cx - z + 1)) + \exp(-in\pi(cx + z - 1))] \quad (4.12)$$

These generate propagating modes in a Fourier series periodic with period $cx = 2$ that are not generally RDF. For the example (3.10), $\hat{h}_1(n\pi)$ is exponentially small with increasing n with measurable radiation only for the lowest modes. Note that in this example, the topography is a Schwartz function. Ambiguities appear to arise from the regularization of $\hat{h}_1(k)/\sin(2\pi k)$ at half-integers, where the use of the principal value is only one choice among many. The results could differ by linear combinations of $\delta(k - n/2)$, producing terms of the form $\exp(\pi i n c x)$ in the inverse Fourier transforms, but such contributions in ψ are precluded by the upper boundary condition.

The question then remains as to whether any RDF solution ψ will exist for an arbitrary compactly supported $h_1(x)$? By way of example, consider the even simpler topography, $h_1(cx) = \varepsilon \operatorname{sech}(\pi c x)$, a Schwartz function, whose transform is also a Schwartz function,

$$\hat{h}_1(k) = \varepsilon \operatorname{sech}(\pi k) \quad (4.13)$$

(Bracewell, 1978) and which, when substituted into Eq. (4.10), gives a radiating field in f , although one that again diminishes rapidly with k . Evidently, to avoid radiation (as discussed briefly by M11), a necessary condition is that $\hat{h}_1(k)$ must have zeros at the pole positions—an artificial construct that surely does not occur in nature. Another, more likely, possibility is that $\hat{h}_1(k)$ has diminished effectively to zero by the position of the smallest non-zero pole at $k = 1/2$, which, consistent with the uncertainty principle, would produce a relatively broad $h_1(cx)$. Such profiles are weakly radiating of high wavenumbers—a wider class than non-radiating solutions, and mainly the lowest modes will be seen in the far-field.

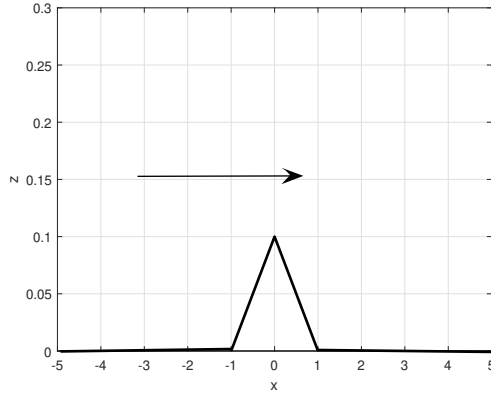


Figure 3: The triangle function $\epsilon\Lambda(cx)$.

5. Corners

Asymptotics

Alternative, and more general, descriptions of topographic influence can be inferred from the Fourier transform asymptotics described e.g., by Lighthill (1958). Those asymptotics can be used to show that most topographies manifesting themselves as a corner, i.e., an abrupt change in slope, (with $\hat{\psi}(k)$ diminishing as k^{-2} for large k), or more rapidly for any higher derivative discontinuity, would in general be radiating. Apart from the abyssal plains, oceanic topographic features short compared to the internal tide-frequency wavelengths—corner-like—are nearly ubiquitous and will thus necessarily be radiators. These will be superimposed upon both perturbation and finite amplitude topographies.

A nonradiating “Corner”

Horizontal wavelengths of low-mode internal tides are tens of kilometers and longer, long compared to numerous topographic features. That configuration raises the question of the effect of a “corner” on a tidal flow, i.e., a point of derivative discontinuity in the topography. Here we consider a corner in which the slopes are subcritical (cf. Hurley, 1972). Consider a non-Schwartz topography $h_1(cx)$ proportional to the triangle function (Fig. 3 and see particularly, Pétrélis et al., 2006),

$$\Lambda(cx/a) = \begin{cases} 0, & |cx/a| > 1 \\ 1 - |cx/a|, & |cx/a| \leq 1 \quad (a > 0) \end{cases}$$

which has compact support. The Fourier transform is

$$\hat{\Lambda}(k) = a \operatorname{sinc}^2(ka) = a \frac{(\sin \pi ka)^2}{(\pi ka)^2}.$$

If $a = 2$, with a bottom perturbation of order $\epsilon \ll 1$, the inverse Fourier transform of f takes the form

$$f(cx) = 4i\epsilon \int_{-\infty}^{\infty} \exp(2i\pi kcx) \frac{\sin(2\pi k)}{(2\pi k)^2} dk \quad (5.1)$$

with ϵ a small parameter, vanishing at all the poles at wavenumbers, $k = n/2$, an accident of the width, and none of the propagating modes is excited. See Fig. 4. Again issues of regularization at $k = 0$ potentially arise, but are generally irrelevant because of the boundary conditions on ψ .

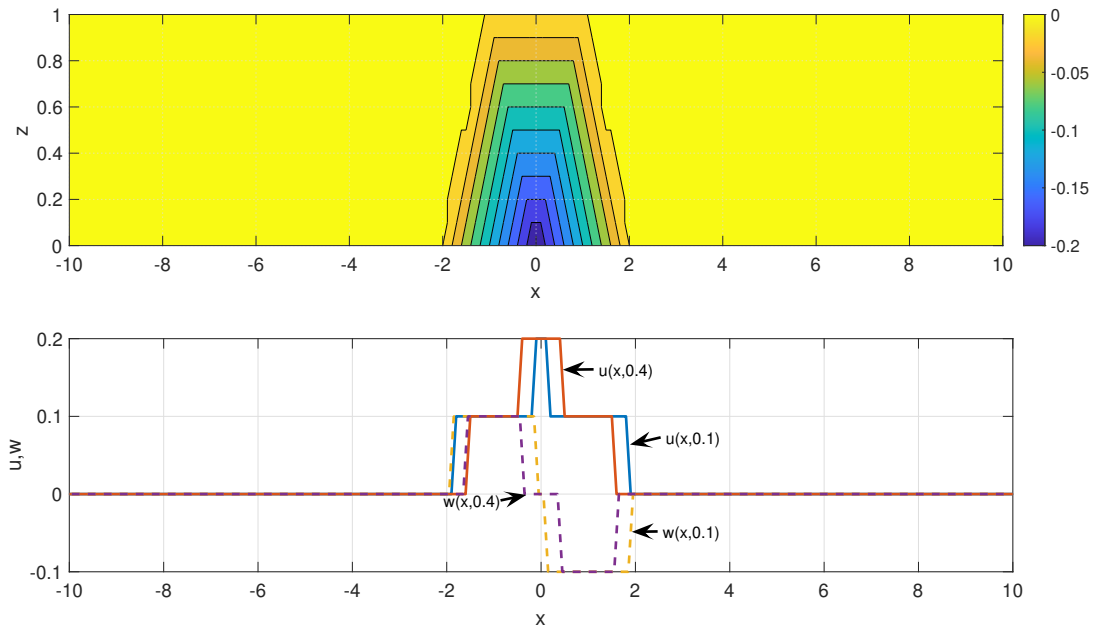


Figure 4: Stream function $\psi(x, z)$ for the triangle function of width 2 (upper panel). u, w at two depths for the triangle function (lower panel).

Alternatively, define a simple ramp as

$$\begin{aligned} G(x) &= -1, \quad x \leq -1/2 \\ &= 2x, \quad -1/2 \leq x \leq 1/2 \\ &= 1, \quad 1/2 \leq x \end{aligned} \quad (5.2)$$

and put,

$$f(cx) = \frac{\varepsilon}{8} G\left(\frac{cx}{2}\right) \quad (5.3)$$

Then, from Eq. (3.1),

$$\psi(cx, z) = \frac{\varepsilon}{8} \left(-G\left(\frac{cx - z + 1}{2}\right) + G\left(\frac{cx + z - 1}{2}\right) \right) \quad (5.4)$$

confined over the region of the ridge but with derivative, and hence velocity, discontinuities at the ramp edges. These would be sites of intense dissipation with corner radiation.

More generally, a corner will typically have asymptotic wavenumber contribution diminishing with k^{-2} in the far-field. The stream function in the vicinity of the corner will be complicated and of high shear. Related numerical solutions are Nie et al. (2019) who computed the solution for the critical case, and Liang and Wunsch (2015) who computed the nonlinear interactions for a double exponential sub-critical ridge in a rotating system.

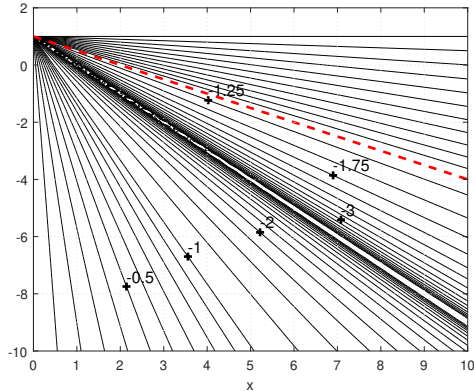


Figure 5: ψ_{wedge} from Eq. (5.5) and a constant slope $\gamma = 0.4$ (dashed red line). Contouring near the singularity at $cx = 0, z = 1$ and along the critical slope $z = cx$ is incomplete. Solution, also shown, would be appropriate *below* the critical line although not oceanographically interesting there.

5.1. Finite Topography-Uniform Slope

M11 noticed that for finite amplitude sub-critical slopes, Eq. (2.2) has a *non-RDF*, solution when forced by a vertically uniform horizontal flow,

$$\psi_{wedge}(cx, z) = \ln\left(\frac{cx - z + 1}{cx + z - 1}\right) = \ln(cx - z + 1) - \ln(cx + z - 1), \quad 0 \leq z \leq 1, x > 0 \quad (5.5)$$

in the present notation, vanishing on $z = 1$ as required and also conserving volume flux in the externally imposed oscillating flow U . ψ_{wedge} must be a constant, along a slope, such that,

$$\frac{cx - z + 1}{cx + z - 1} = \beta,$$

where β is a constant or,

$$z = \gamma cx + 1, \quad \gamma = \left(\frac{1 - \beta}{1 + \beta}\right) < c, x > 0$$

with a zero-depth corner at $x = 0, z = 1$ (Fig. 5) where the equations fail.

This solution is valid for finite amplitude subcritical topography, under an imposed oscillating flow with magnitude increasing monotonically as the zero-depth corner is approached from $x < 0$. No radiating linear waves are generated, albeit if the slope region is finite—as is physically necessary—then the transitions to a flat bottom in both deep water and prior to the corner would have $\partial h_1 / \partial (cx)$ discontinuous. A radiated far-field, with Fourier transform again falling as k^{-2} , will be generated there. Solutions (5.5) might have some applicability over the large-scale sloping abyssal plains.

A topographic perturbation to a uniform slope can be dealt with in a form analogous to that done for perturbations to a flat bottom (cf. the treatment in M11 via coordinate transformation). Let $h = h_0 + h_1$, where $h_0 = \gamma cx + 1$ and h_1 is a perturbation. Let $\mathbf{u} = (u, w) = \mathbf{u}_0 + \mathbf{u}_1$, where \mathbf{u}_0 corresponds to the undisturbed stream function Eq. (5.5). Then to lowest order the boundary condition becomes,

$$\mathbf{u} \cdot \nabla (h - z)|_{z=\gamma x+1} \approx \mathbf{u}_0|_{z=\gamma x+1} \cdot \nabla h_1 + \mathbf{u}_1|_{z=\gamma x+1} \cdot \nabla (h_0 - z) = 0 \quad (5.6)$$

Letting $\mathbf{u}_1 = (\partial \psi_1 / \partial z, -\partial \psi_1 / \partial x)$, ψ_1 must satisfy the same governing hyperbolic equation

as ψ . With $\nabla(h_0 - z) = (\gamma, -1)$, hence with f_1 as in (3.1), the boundary condition is

$$(1 - \gamma)f_1'((1 - \gamma)cx) - (1 + \gamma)f_1'((1 + \gamma)cx) = -\mathbf{u}_0|_{z=\gamma x+1} \cdot \nabla h_1 = Q'(cx) \quad (5.7)$$

In the limit $\gamma \rightarrow 0$, the slope coincides with the upper boundary.

The natural integral transform for wedge-geometries is the Mellin transform (Sneddon, 1972) and thus defining

$$f_1^{(\text{Mln})}(s) = \mathcal{M}(f_1')(s) = \int_0^\infty q^{s-1} f_1'(q) dq \quad (5.8)$$

with inverse transform,

$$f_1'(cx) = \frac{1}{2\pi i} \int_{\beta-i\infty}^{\beta+i\infty} f_1^{(\text{Mln})}(s) (cx)^{-s} ds \quad (5.9)$$

for some constant β , and with corollary,

$$\mathcal{M}(f_1')(\alpha x) = \alpha^{-s} f_1^{(\text{Mln})}(s). \quad (5.10)$$

Applying $\mathcal{M}(\cdot)$ to Eq. (5.7)

$$\begin{aligned} \frac{1}{(1 - \gamma)^{s-1}} f_1^{(\text{Mln})}(s) - \frac{1}{(1 + \gamma)^{s-1}} f_1^{(\text{Mln})}(s) &= \mathcal{M}(Q'(cx)) \\ f_1^{(\text{Mln})}(s) &= \frac{(1 - \gamma)^{s-1} (1 + \gamma)^{s-1}}{(1 + \gamma)^{s-1} - (1 - \gamma)^{s-1}} \mathcal{M}(Q'(cx)) \end{aligned} \quad (5.11)$$

for any Mellin transformable $Q'(cx)$. The logarithmic singularity implicit here means that there is no equivalent of the Schwartz function solutions. These topographies are not pursued further here. The free *propagating* modes in this finite slope configuration (Wunsch, 1969) can be added with arbitrary amplitudes.

6. Summary

The determination of subcritical topography without ‘tidal conversion,’ discussed by Maas (2011), can be found from a formulation in the linearized case not involving conformal-mapping analogues. As with his solutions, choice of a rapidly decaying stream function leads readily to a determination of a corresponding bottom topography, $h_1(cx)$ in an inverse problem. All solutions *over* the topography can be intense, with quantitative implications for ocean mixing, whether the topography is a radiating one or not. Direct solution of a governing functional equation (Manton and Mysak, 1971) permits generation of an infinite number of non-radiating topographies for a tidal disturbance at a fixed frequency. The wider class of Schwartz function topographies are poor radiators of high wavenumber fields.

Constraints on non-radiating topography are so great however, that their appearance outside the laboratory or the computer seems very unlikely. One useful interpretation is that a solution at one non-radiating tidal frequency ω will, if the forcing is changed to another tidal frequency, generally produce radiation. Thus in moving from the period of the principal lunar tide, M_2 at 12.42 hours to that of the principal solar tide, S_2 at 12.0 hours (e.g., Zhao, 2017), the M_2 null space will vanish.

The inverse problem of determining $h_1(cx)$ from far-field measurements will be non-unique up to topographic structures that are non-radiating (or below noise levels); see the Appendix. Primary concern will be less the inability to determine those structures, and more the necessity of observations to estimate mixing confined closely to the topography itself.

The class of non-converting topographies appears to be extremely fragile and unlikely to be found in oceanographic practice.

Practical utility aside, numerous interesting theoretical extensions of this problem remain: general finite amplitude topography, super-critical-reflective slopes and corners, three-dimensions with rotation, non-constant $N(z)$, non-linear interactions, shear flows, diffusion, dissipation, transient establishment, and stochastic forms of topography and values of U , all remain to be explored.

Appendix A. Inversion with Observations

The inverse problem with observations has a different flavor from the purely theoretical discussion above. As an example, let w (Eq. 3.2) be measured at M positions x_i, z_i with some error n_i with known first and second moments. (w would likely be inferred from a measurement of temperature, with the mean vertical temperature gradient being used to calculate the vertical displacement through time.) Put $r_i = cx_i - z_i + 1$, $s_i = cx_i + z_i - 1$. Then measure $w(x_i, z_i)$, defined as $y_i = w_i + n_i$ where n_i is the noise. Eqs. (4.5) are a set of linear equations for the slopes and whose solutions $h'_1(r_i), h'_1(s_i)$ can be estimated by conventional linear algebraic methods for M -equations in $2m + 1$ -unknowns. To the degree the problem is underdetermined, a null-space in the elements $h'_1(q_i)$ will result. From an estimate of h'_1 , h_1 itself can be estimated with computable uncertainty.

In practice, other procedures may be more convenient. For example, scale the domain consisting of $\min(r_i, s_i) \leq \{r_i, s_i\} \leq \max(r_i, s_i)$ to lie between $-1 \leq \{r'_i, s'_i\} \leq 1$, and expand the unknown,

$$f(r'_i) = \sum_{m=1}^M a_m T_m(r'_i) \quad (\text{A } 1)$$

where, somewhat arbitrarily, the T_m are the ordinary Chebyshev polynomials. Then

$$\begin{aligned} y_i &= w_i(x'_i, z'_i) + n_i = -f'(r'_i) + f'(s'_i) \\ &= \sum_{m=1}^M a_m (T_m(s'_i) - T_m(r'_i)) \end{aligned} \quad (\text{A } 2)$$

and which is readily solved by conventional least-squares/Gauss-Markov methods for estimates of a_m with values dependent upon the statistics of n_i . Evidently, any complete set of functions can be used. (Note that as written, the T_m are not orthogonalized over the present data interval.)

The result for $f'(x)$ from using $T_m, m = 1, \dots, 30$ and a 10% added white noise at each point can be seen in Fig. 6. In practice, one would likely control the ripple by use of a prior structure on f' , but this artificial example is not further pursued here as the principle is clear. An estimate of f' leads to a corresponding estimate of $h'(cx)$, compared to the true value in Fig. 7. The full analysis yields uncertainty estimates for h' as well as resolution estimates both on the individual data points and on the Chebyshev coefficients—not shown.

Eq. (4.5) implies that slope contributions from infinitely distant points contribute to the local measurement—a plausible result only for a purely inviscid situation. Should such an inverse problem be attempted in practice, a prior estimate of h'_1 with some estimate of its uncertainty would normally be available, along with an estimate of the extent to which distant contributions would be dissipated. Although the inverse machinery permits understanding of the error covariances and the resolution of the solution and of the different data positions, further exploration of this hypothetical problem is omitted here. In fully radiating situations,

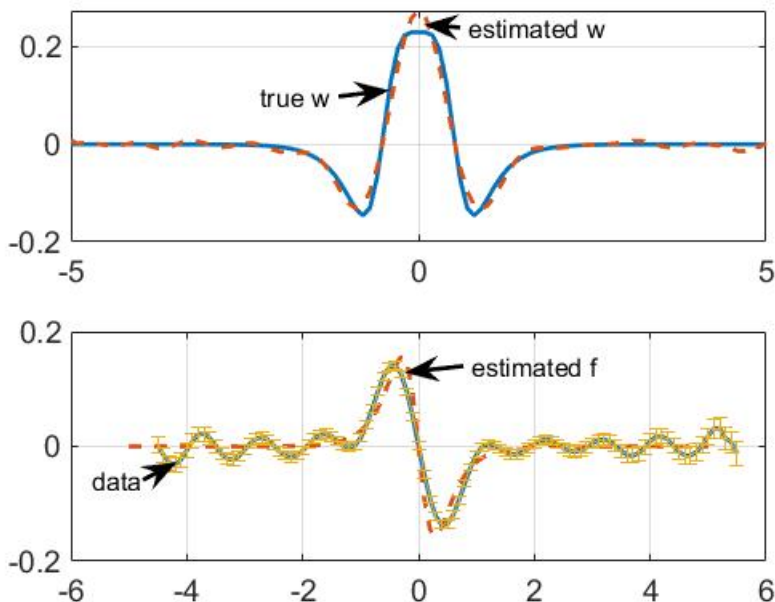


Figure 6: (Upper panel) Exact w at $z = 0.5$ for the same topography as in Fig. 1 and the result of inverting it with "data" having standard deviation of 10% of the Chebyshev polynomials for an expansion using $m = 1, \dots, 30$. Assumption is of white noise. (Lower panel). Inferred and correct value of $f(x)$ from using $w(x, z = 0.5)$. Error bars are one standard deviation. Correct value of f is shown as a solid line.

the existence of a ‘near-field’ over the topography is of intense oceanographic interest for its implications about large-scale mixing. Note only that the effective null space of the topography in this formulation consists of the higher wavenumber Chebyshev polynomials.

Linear in situ array measurements of baroclinic tidal amplitudes are rare. Much more common are global estimates of surface elevation, ζ , owing primarily, but not wholly, to the first baroclinic mode (Zhao et al. 2016). Surface pressure, $p(x, z = 1) = g\rho\zeta(x)$, (exerted against the rigid lid), is related to the stream function through the dimensional equations,

$$-\frac{\partial p}{\partial x} = \frac{\omega^2 - f^2}{i\omega} \frac{\partial \psi}{\partial z} \quad (\text{A } 3a)$$

$$-\frac{\partial p}{\partial z} = \frac{N^2 - \omega^2}{i\omega} \frac{\partial \psi}{\partial x} \quad (\text{A } 3b)$$

and this opens the novel possibility of inferring generating topography from altimetric data.

Acknowledgements. We appreciate numerous comments and corrections by by L. R. M. Maas, H. van Haren, L. Mysak, the editor O. Bühler, and three referees.

Funding. Supported in part (JW) by Simons Foundation grant 631302, NSF grant DMS–2054424, and a Simons Fellowship; and (CW) in part by the Cecil and Ida Green Professorship at MIT.

Declaration of interests. .

The authors report no conflict of interest.

Data availability statement. No observational data were used in this study.

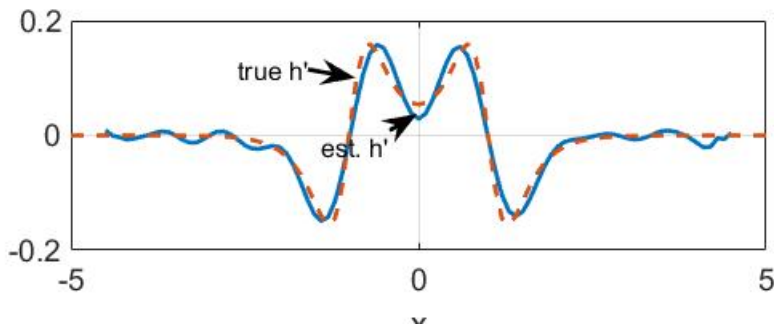


Figure 7: Estimated topography slope using a rank $M = 30$ Chebyshev polynomial expansion with noise. Error estimate (not shown) accounts for the covariance in the errors of $f'(x + 1)$ and $f'(x - 1)$.

Author ORCID. C. Wunsch, <https://orcid.org/0000-0001-6808-3664>; J. Wunsch, <https://orcid.org/0000-0009-8765-4321>

References

- Aczél, J. (1966). *Lectures on Functional Equations and their Applications*. New York, Academic Press.
- Bahret, W. F. (1993). The beginnings of stealth technology *IEEE Trans. Aerospace and Electronic Systems* 29: 1377–1385.
- Baines, P. G. (1973). Generation of internal tides by flat-bump topography *Deep-Sea Res.* 20: 179–205.
- Balazs, N. L. (1961). On the solutions of the wave equations with moving boundaries *J. Math. Anal. Appl.* 3: 472–484.
- Balmforth, N., J. G. R. Ierley, W. R. Young (2002). Tidal conversion by subcritical topography. *J. Phys. Oc.*, 32: 2900–2914.
- Beckebanze, F. and G. Keady (2016). On functional equations leading to exact solutions for standing internal waves. *Wave Motion* 60: 181–195.
- Bracewell, R. N. (1986). *The Fourier Transform and Its Applications*. New York, McGraw-Hill.
- Bühler, O. and M. Holmes-Cerfon (2011). Decay of an internal tide due to random topography in the ocean. *J. Fluid Mech.* 678: 271–293.
- Cheney, E. W. (2001). *Analysis for Applied Mathematics*. New York, Springer.
- Colin De Verdiere, Y. and L. Saint-Raymond (2020). *Attractors for Two-Dimensional Waves*

- with Homogeneous Hamiltonians of Degree 0. *Communications on Pure and Applied Mathematics*, 73: 421–462.
- Dyatlov, S., and M. Zworski (2019). Microlocal analysis of forced waves. *Pure and Applied Analysis*, 1: 359–384.
- Cox, C. and H. Sandstrom (1962). Coupling of internal and surface waves in water of variable depth. *J. Oceanog. Soc. Japan* 18: 499–513.
- Garrett, C. and E. Kunze (2007). Internal tide generation in the deep ocean. *Ann. Rev. Fluid Mechs.* 39: 57–87.
- Gordon, C. and D. Webb (1996). You can't hear the shape of a drum. *Am. Sci.*, 84: 46–55.
- Greenspan, H. P. (1963). A string problem. *J. Math. Anal. and Appl.* 6: 339–348.
- Hazewinkel, J., C. Tsimitri, L. R. M. Maas, S. B. Dalziel (2010). Observations on the robustness of internal wave attractors to perturbations. *Phys. Fl.* 22, 107102.
- Hurley, D. G. (1972). General method for solving steady-state internal gravity wave problems. *J. Fluid Mech.* 56: 721–740.
- Kac, M. (1966). Can one hear the shape of a drum? *Am. Math. Monthly* 73: 1–23.
- Kadec, M., T. Bückmann, R. Schittny, M. Wegener (2015). Experiments on cloaking in optics, thermodynamics and mechanics. *Phil. Trans. R. Soc. Lond. A.* 373: 1–20.
- Liang, X. and C. Wunsch (2015). Note on the redistribution and dissipation of tidal energy over mid-ocean ridges. *Tellus A* 67: 1–9.
- Lighthill, M. J. (1958). *Fourier Analysis and Generalized Functions*, Cambridge Un. Press.
- Llewellyn Smith, S. G. and W. Young (2002). Conversion of the barotropic tide. *J. Phys. Oc.* 32: 1554–1566.
- Llewellyn Smith, S. G. (2011). A conundrum in conversion. *J. Fluid Mech.* 684: 1–4.
- Maas, L. R. M. (2011). Topographies lacking tidal conversion. *J. Fluid Mech.* 684: 5–24.
- Maas, L. R. M. and U. Harlander (2011). Tide topography interaction?. *Proc. 7th International Symp. on Stratified Flows*, Rome, Italy, Aug. 22–26: 1–8.
- Magaard, L. (1962) Zur Berechnung interner Wellen in Meeresräumen mit nicht-ebenen Böden bei einer speziellen Dichteverteilung. *Open Access Kieler Meeresforschungen*, 18: 161–183.
- Manton, M. J. and L. A. Mysak (1971). Construction of internal wave solutions via a certain functional equation. *J. Math. Anal. Appl.* 35: 237–248.
- Morozov, E. G. (2018). *Oceanic Internal Tides: Observations, Analysis and Modeling*, Springer International, Cham, Switzerland.
- Nie, Y. H., Z. W. Chen, and 4 others. (2019). Internal waves generated by tidal flows over a triangular ridge with critical slopes. *J. Ocean Un. China* 18: 1005–1012.
- Pétrélis, F., S. Llewellyn Smith, and W. Young (2006). Tidal conversion at a submarine ridge. *J. Phys. Oc.* 36: 1053–1071.
- Poincaré, H. (1885). Sur l'équilibre d'une masse fluide animée d'un mouvement de rotation. *Acta Mathematica* 7: 259–380.
- Ray, R. D. and G. T. Mitchum (1997). Surface manifestation of internal tides in the deep ocean: observations from altimetry and island gauges. *Prog. Oceanog.* 40: 135–162.
- Sandstrom, H. (1975). On topographic generation and coupling of internal waves. *Geophys. Fluid Dyn.* 7: 231–270.
- Sneddon, I. N. (1972). *The Use of Integral Transforms*, McGraw-Hill, New York.
- Stratton, J. A. (1941). *Electromagnetic Theory*. New York, London, McGraw-Hill book company, inc.
- Wunsch, C. (1969). Progressive internal waves on slopes. *J. Fluid Mech.* 35: 131–145.
- Zhao, Z. (2017). The global mode-1 S2 internal tide. *J. Geophys. Res.: Oceans* 122: 8794–8812.
- Zhao, Z., M. H. Alford, J. B. Girton, L. Rainville, H. L. Simmons (2016). Global observations of open-ocean mode-1 M2 internal tides. *J. Phys. Oc.* 46: 1657–1684.